Collapse of hard-axis behavior in uniaxial Co films

O. Idigoras,[1] A. K. Suszka,[1,*] P. Vavassori,[1,2] P. Landeros,[3] J. M. Porro,[1] and A. Berger[1]
[1]*CIC nanoGUNE Consolider, E-20018 Donostia-San Sebastian, Spain*
[2]*IKERBASQUE, The Basque Foundation for Science, 48011 Bilbao, Spain*
[3]*Departamento de Física, Universidad Técnica Federico Santa María, Avenida España 1680, 2390123 Valparaíso, Chile*
(Received 17 July 2011; published 4 October 2011)

We study the magnetic properties of weakly disordered Co films with in-plane uniaxial magnetocrystalline anisotropy. The growth sequence used allowed the controlled introduction of grain orientation disorder. Above a threshold disorder level, we observe an anomalous magnetic reversal near the nominal hard axis; while the behavior in all other field orientations is barely affected. A two-grain model explains the anomaly as the occurrence of nonuniform magnetization states near the hard axis, a fact that is experimentally confirmed by Kerr microscopy.

DOI: 10.1103/PhysRevB.84.132403 PACS number(s): 75.30.Gw, 75.60.Jk, 75.70.Ak

The presence or absence of crystallographic order is crucial for magnetic properties of materials due to the magnetocrystalline anisotropy that originates from the quantum mechanical spin-orbit coupling.[1–4] Its importance is equally relevant for fundamental properties and technical applications of ferromagnetism. For instance, ferromagnetism is only made possible in two-dimensional systems, e.g., ultrathin films, due to the existence of uniaxial anisotropy,[5] which circumvents the "spin-wave catastrophe" of the Mermin-Wagner theorem.[6] Magnetocrystalline anisotropy is also essential for nonvolatile data storage applications, where it defines the stability of data pattern and ultimately determines the viability of this technology.[7,8] The influence of crystallographic order on magnetocrystalline anisotropy has been extensively studied in terms of identifying and modifying it,[9–13] as well as measuring its influence onto phase transitions,[14–16] spin-wave properties,[17,18] or nanoscale magnetization structures.[19–21] However, most studies of magnetocrystalline effects have been either focused on fundamental properties utilizing the highest possible degree of sample crystallinity or dedicated to technical ferromagnetic materials with relatively high disorder, e.g., recording media.[22] Correspondingly, rather little is known about ferromagnets in the intermediate regime, starting with slight deviations from "perfect" crystalline order up to strongly disordered materials.

In the current work, we specifically studied the regime of relatively low disorder, in which magnetic properties are still dominated by anisotropic behavior. For this purpose, we devised a procedure that allowed for a precise tuning of crystalline order in uniaxial Co films by partial interruption of epitaxy. Our Co films were fabricated by sputter deposition in ultra-high-vacuum onto hydrofluoric acid–etched Si(110) substrates. The growth sequence to achieve good epitaxy with an in-plane hexagonal close packed (hcp) *c*-axis was Ag 75 nm/Cr 50 nm/Co 30 nm/SiO_2 10 nm. It was previously shown that a Ag/Cr bilayer grown epitaxially onto a single-crystal Si(110) substrate serves as an appropriate template for highly oriented (hcp) Co(10$\bar{1}$0) thin films,[23] resulting in the epitaxial sequence Si(110)/Ag(110)/Cr(211)/Co(10$\bar{1}$0) (Fig. 1). Our specific growth process was optimized in terms of deposition rate, pressure, and temperature to achieve the highest magnetic orientation ratio,[24] i.e., the highest degree of uniaxial magnetic alignment. In addition to highly epitaxial Co films, we fabricated partially epitaxial films by slightly disturbing the growth sequence in a well-defined and controlled manner. Specifically, we introduced an ultrathin Si-oxide layer of defined thickness in the order of a single monolayer on top of the Si substrate prior to the Ag-film growth. A set of 20 samples with varying SiO_2 onset-layer thickness was grown. In the current work, we show only the most significant results, which span samples with 0, 1.1, 1.32, and 1.65 Å of SiO_2 onset-layer thickness, labeled as samples A, B, C, and D, respectively. All samples in this study also have a 10-nm-thick SiO_2 overcoat, grown on top of the Co film, to avoid oxidation and aging under ambient conditions.

Figure 1 shows high-angle θ–2θ x-ray diffraction measurements for the epitaxial sample A (dashed line) in comparison to the partially epitaxial sample C (solid line). The deposited SiO_2 onset-layer thickness clearly influences the overall crystallographic structure and causes a decrease of the Co(10$\bar{1}$0) peak intensity. For sample C, we also observed the appearance of Ag(111) and Ag(311) peaks, which indicate a partial loss of the epitaxy-induced Ag(110) orientation, even though a quantitative analysis of the relative peak heights confirmed that this sample is by no means random but still has a preferred (110) texture. In addition, we performed rocking curve measurements of the Co(10$\bar{1}$0) peak, whose results are tabulated in Fig. 1. We found a continuous increase of the Co(10$\bar{1}$0) peak width upon increasing the SiO_2 onset-layer thickness, indicating a continuous decrease of lateral crystallographic alignment and correlation. By decorating the Si single-crystal surface, the SiO_2 locally interrupts the epitaxial growth of the Ag layer. This partial loss of epitaxy is then transferred to the subsequently deposited layers, including the magnetic Co film. By atomic force microscopy, we also measured the sample roughness but could not detect any significant change upon introducing the SiO_2 onset layer, indicating that it is predominantly the crystallographic structure that is modified here.

Angular-dependent in-plane hysteresis loops were measured using a longitudinal magneto-optical Kerr effect (MOKE) setup. The magnetic field was applied in the film plane, and loops were recorded as a function of the in-plane field angle β between the applied magnetic field and the easy axis (*EA*). Detailed micromagnetic structures were also investigated using an Evico Kerr microscope in longitudinal geometry. Figures 2(a)–2(d) show MOKE hysteresis loops

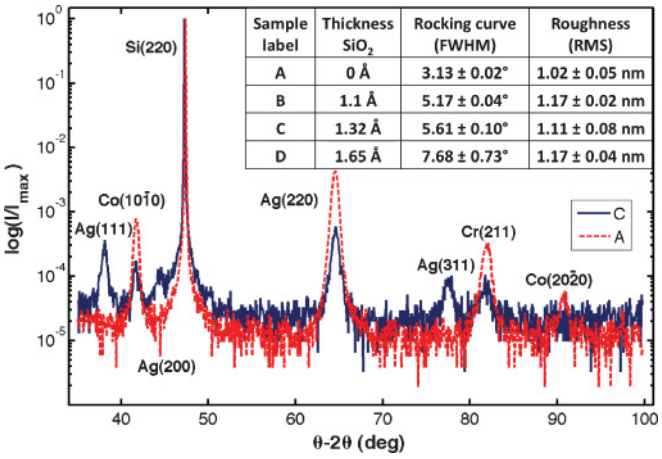

Sample label	Thickness SiO_2	Rocking curve (FWHM)	Roughness (RMS)
A	0 Å	3.13 ± 0.02°	1.02 ± 0.05 nm
B	1.1 Å	5.17 ± 0.04°	1.17 ± 0.02 nm
C	1.32 Å	5.61 ± 0.10°	1.11 ± 0.08 nm
D	1.65 Å	7.68 ± 0.73°	1.17 ± 0.04 nm

FIG. 1. (Color online) High-angle x-ray diffraction (θ–2θ) scan for the epitaxial film sample A (dashed red line) and sample C with partially suppressed epitaxy (solid blue line). The inset provides a table with key sample characteristics, e.g., its name; the SiO_2 onset-layer thickness; the Co(10$\bar{1}$0) rocking curve width, given as the full width at half maximum; and the root-mean-square surface roughness.

for the fully epitaxial sample A without an SiO_2 underlayer, in comparison to results for sample C, which are shown in Figs. 2(e)–2(h). The *EA* hysteresis loops in Figs. 2(a) and 2(e) show similar rectangular loop shapes with high remanence and abrupt magnetization reversal for both samples. Figures 2(b) and 2(f) and Figs. 2(d) and 2(h) show hysteresis loops $\pm 2^\circ$ away from the nominal hard axis (*HA*) direction. Here, a hysteretic behavior is nearly absent for both samples, which is the expected behavior for samples with a high degree of crystalline orientation. Figures 2(c) and 2(g) show

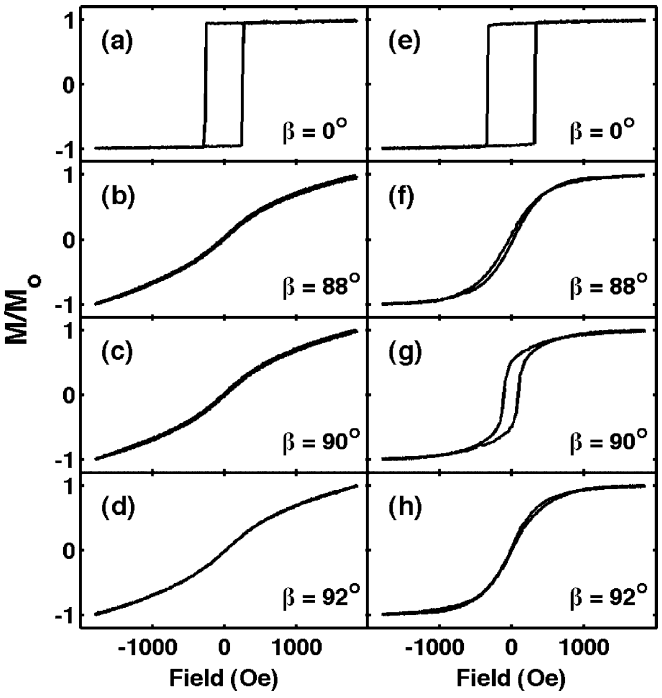

FIG. 2. MOKE hysteresis loops for (a)–(d) sample A and (e)–(h) sample C for different orientations β of the applied in-plane magnetic field.

magnetization reversal along the nominal *HA*, for which we observe a substantial difference between the two samples. While the epitaxial sample shows the expected hysteresis-free *HA* loop, the partially ordered sample C exhibits an unexpected behavior, i.e., a loop that shows substantial values of coercive field H_c and remanent magnetization M_r. Thus, for sample C, the magnetic reversal in the nominal *HA* does not show typical *HA* behavior anymore. Anomalies of magnetization reversal in the proximity of the nominal *HA* direction were previously reported for a few magnetic materials.[25–28] The corresponding results were explained by several mechanisms, including local magnetic frustrations of adjacent domains[25] or local lattice expansions.[28] In general, the observed anomaly effects were small and no sufficient structural control of the samples was available so that overall no consistent and satisfactory physical picture of these anomalies could be deduced.

To study this anomaly in more detail, Figs. 3(a)–3(d) show the angular dependence of the normalized remanent magnetization (M_r/M_0) for samples with different SiO_2 onset-layer thicknesses. The epitaxial sample, Fig. 3(a), shows the expected uniaxial characteristics, following closely a $|\cos(\theta)|$ behavior, which corresponds to the geometric projection of the *EA* magnetization onto the field axis. Virtually the same characteristics were observed for sample B in Fig. 3(b). Samples C and D, presented in Figs. 3(c) and 3(d), respectively, show related characteristics for most of the β range, with the exception of the nominal *HA* and its immediate vicinity. Corresponding to the loop shapes of Figs. 2(f)–2(h), M_r exhibited a sharp and pronounced peak as a function of β that was centered at the nominal *HA*. The peak increased its width and height as we increased the disorder in the structure, i.e., by moving from sample C to sample D.

To develop a qualitative understanding of the observed *HA* anomaly, we devised a two-grain Stoner-Wohlfarth model with intergranular exchange coupling and grain axis misalignment. Its energy is given by

$$E = -J\vec{m}_1 \cdot \vec{m}_2 - \vec{H}(\vec{m}_1 + \vec{m}_2) - \tfrac{1}{2}K_1(\vec{m}_1 \cdot \vec{n}_1)^2 - \tfrac{1}{2}K_2(\vec{m}_2 \cdot \vec{n}_2)^2, \quad (1)$$

where J is the intergranular exchange coupling constant between the two grains characterized by their respective magnetization vectors $\vec{m}_1$ and $\vec{m}_2$ and their respective magnetocrystalline easy axes are given by the unit vectors $\vec{n}_1$ and $\vec{n}_2$. The magnetocrystalline anisotropy constants K_1 and K_2 are assumed to be identical here because neighboring grains are made of pure Co. Similar models had been used successfully to describe magnetization reversal in films that exhibited a combination of uniaxial and fourfold magnetocrystalline anisotropy.[29] Due to the strong demagnetizing effect of the thin film geometry, and a magnetocrystalline anisotropy, which has the *c*-axis on average aligned within the surface plane, we can further modify Eq. (1) by restricting $\vec{m}_1$ and $\vec{m}_2$ to the *xy*-surface plane, which we also assume to contain the two *EA* vectors $\vec{n}_1$ and $\vec{n}_2$.[30] Under these conditions, we find

$$E = -J\cos(\theta_1 - \theta_2) - H[\cos(\theta_1 - \beta) + \cos(\theta_2 - \beta)] - \tfrac{1}{2}K_1[\cos^2(\theta_1 - \omega/2) + \cos^2(\theta_2 + \omega/2)], \quad (2)$$

where θ_1, θ_2, and β are the in-plane orientation angles of $\vec{m}_1$, $\vec{m}_2$, and $\vec{H}$, respectively, in reference to the average anisotropy

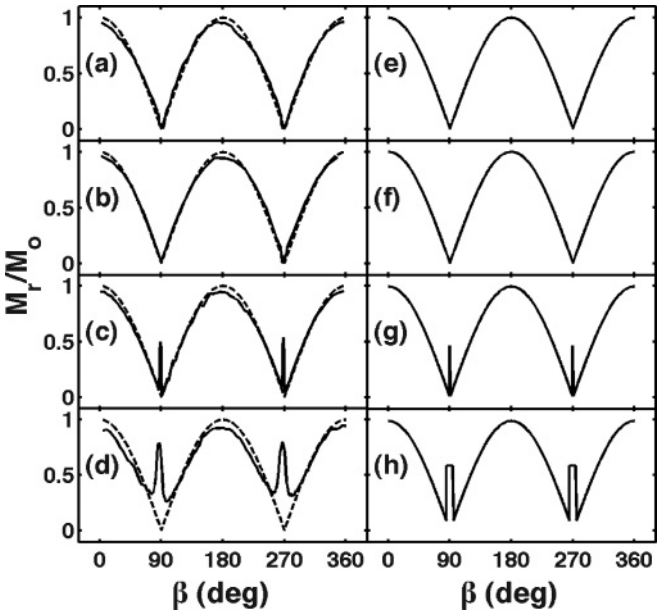

FIG. 3. (a)–(d) Angular dependence of M_r/M_0 for the four samples: (a) A, (b) B, (c) C, and (d) D. The solid lines are experimental M_r/M_0 data, while the dashed lines are the geometric projection of the *EA* magnetization onto the applied field axis, i.e., the perfect Stoner-Wohlfarth-model case. (e)–(h) The calculated angular dependence of M_r/M_0 for the misaligned two-grain model according to Eq. (2), assuming $J/K_1 = 0.35$ and different values of ω: (e) $\omega = 0°$, (f) $\omega = 10°$, (g) $\omega = 20°$, and (h) $\omega = 30°$.

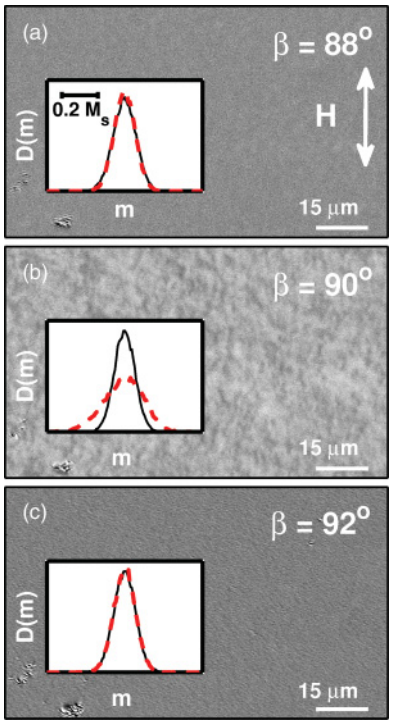

FIG. 4. (Color online) Kerr microscopy images of sample C, with the magnetic field applied: (a) $-2°$ from, (b) along, and (c) $+2°$ from the nominal *HA*. The inset figures show the brightness distributions $D(m)$ of the Kerr images in saturation (solid thin black line) and in remanence (dashed thick red line). The brightness m is hereby proportional to the local magnetization value after the subtraction of the picture average, i.e., $m \sim M - \langle M \rangle$. The proportionality constant has been determined from saturation experiments and is represented by the scale in (a).

axis. ω is the misalignment angle between the two grains. From Eq. (2), it is evident that the magnetization reversal behavior depends on the field angle β and the material-specific parameters J/K_1 and ω.

We simulated the process of magnetization reversal in this two-grain system starting from high-field saturation by stepwise field reduction to zero. Figures 3(e)–3(h) show simulated $M_r/M_0(\beta)$ data for a fixed ratio of $J/K_1 = 0.35$ and varying ω. Up to a certain critical misalignment value ω_c, the two-grain system is virtually identical in its behavior to a single Stoner-Wohlfarth grain, with nearly full M_r along the *EA* and vanishing M_r along the nominal *HA*. In this regime, the exchange coupling energy outweighs the misalignment of the anisotropy axes so that both magnetizations exhibit the same rotation sense for magnetization processes, even near the nominal *HA*. However, above ω_c, or if J/K_1 falls below a certain threshold for fixed ω, there exists a β range in the vicinity of the nominal *HA* in which $\vec{m}_1$ and $\vec{m}_2$ exhibit an opposite rotation sense upon external field reduction. This behavior occurs because the nearest *EA* orientations are nearly antialigned and exchange coupling is too weak to force both magnetizations into a collective rotation. Upon approaching remanence, this scenario leads to a V-like magnetization state, which causes nonvanishing M_r values along or near the nominal *HA*. The corresponding remanence peaks in Figs. 3(g) and 3(h) are qualitatively identical to what is observed experimentally, including an increase and widening of the peak upon increasing ω. The quantitative differences between the experimental data and our simple model can be easily understood because in our two-grain model we study only one specific V-state, while our extended experimental system has many different misalignment angles between neighboring grains. Given a distribution of misalignment angles, the fraction of populated V-states would change with the distribution width and β, resulting in a more substantial increase of the anomalous M_r peak height upon increasing the overall grain misalignment, which is what we observe experimentally.

Following the preceding explanation, the model predicts that the anomaly is characterized by a nonuniform remanent magnetization state. Figure 4 shows Kerr microscopy images of different remanent states for sample C. The remanent states for field orientations $\pm 2°$ from the nominal *HA* are shown in Figs. 4(a) and 4(c). Here, no domains are visible in remanence. However, if the field is applied along the nominal *HA*, as shown in Fig. 4(b), we can clearly observe a nonuniform spatial distribution of magnetization. Hereby, all Kerr images have been measured with the same contrast setting. The insets of Fig. 4 compare the contrast distributions for the different remanent and respective saturated states. For the misaligned field cases, i.e., Figs. 4(a) and 4(c), the distributions are identical for the saturated and the remanent states, whereas there is a clear widening of the contrast distribution in remanence for the nominal *HA* case in Fig. 4(b), which corresponds to $8 \pm 0.7\%$ of M_S.[31] Thus, our Kerr microscopy measurements confirm the existence of an anomalous nonuniform magnetization state

along the nominal *HA*. We have not observed this state in samples with a high degree of epitaxial order, i.e., samples A and B of this work.

We acknowledge funding from the Basque government under Program Nos. PI2009-17, BFI09.284, and BFI09.289 and from the Spanish Ministry of Science and Education under Project No. MAT2009-07980. P. L. acknowledges support from Fondo Nacional de Desarrollo Científico y Tecnólogico Project No. 11080246 and Centro para el Desarrollo de la Nanociencia y la Nanotecnología Project No. FB0807. We acknowledge O. Hovorka for the active discussion.

*a.suszka@nanogune.eu

[1] P. Bruno, Phys. Rev. B **39**, 865 (1989).
[2] D. Weller, J. Stohr, R. Nakajima, A. Carl, M. G. Samant, C. Chappert, R. Megy, P. Beauvillain, P. Veillet, and G. A. Held, Phys. Rev. Lett. **75**, 3752 (1995).
[3] P. Gambardella, S. Rusponi, M. Veronese, S. S. Dhesi, C. Grazioli, A. Dallmeyer, I. Cabria, R. Zeller, P. H. Dederichs, K. Kern, C. Carbone, and H. Brune, Science **300**, 1130 (2003).
[4] J. V. Barth, G. Costantini, and K. Kern, Nature **437**, 671 (2005).
[5] M. Bander and D. L. Mills, Phys. Rev. B **38**, 12015 (1988).
[6] N. D. Mermin and H. Wagner, Phys. Rev. Lett. **17**, 1133 (1966).
[7] D. Weller and A. Moser, IEEE Trans. Magn. **35**, 4423 (1999).
[8] B. D. Terris and T. Thomson, J. Phys. D Appl. Phys. **38**, R199 (2005).
[9] B. N. Engel, C. D. England, R. A. VanLeeuwen, M. H. Wiedmann, and C. M. Falco, Phys. Rev. Lett. **67**, 1910 (1991).
[10] G. H. O. Daalderop, P. J. Kelly, and F. J. A. den Broeder, Phys. Rev. Lett. **68**, 682 (1992).
[11] A. Berger, U. Linke, and H. P. Oepen, Phys. Rev. Lett. **68**, 839 (1992).
[12] W. Weber, A. Bischof, R. Allenspach, C. Wursch, C. H. Back, and D. Pescia, Phys. Rev. Lett. **76**, 3424 (1996).
[13] P. Gambardella, A. Dallmeyer, K. Maiti, M. C. Malagoli, S. Rusponi, P. Ohresser, W. Eberhardt, C. Carbone, and K. Kern, Phys. Rev. Lett. **93**, 077203 (2004).
[14] D. P. Pappas, K.-P. Kamper, and H. Hopster, Phys. Rev. Lett. **64**, 3179 (1990).
[15] M. Farle, Rep. Prog. Phys. **61**, 755 (1998).
[16] D. Sander, J. Phys. Condens. Matter **16**, R603 (2004).
[17] P. Krams, F. Lauks, R. L. Stamps, B. Hillebrands, and G. Guntherodt, Phys. Rev. Lett. **69**, 3674 (1992).
[18] M. Grimsditch, E. E. Fullerton, and R. L. Stamps, Phys. Rev. B **56**, 2617 (1997).
[19] R. P. Cowburn, A. O. Adeyeye, and M. E. Welland, Phys. Rev. Lett. **81**, 5414 (1998).
[20] A. Wachowiak, J. Wiebe, M. Bode, O. Pietzsch, M. Morgenstern, and R. Wiesendanger, Science **298**, 577 (2002).
[21] G. Leaf, H. Kaper, M. Yan, V. Novosad, P. Vavassori, R. E. Camley, and M. Grimsditch, Phys. Rev. Lett. **96**, 017201 (2006).
[22] D. Weller, A. Moser, L. Folks, M. E. Best, W. Lee, M. F. Toney, M. Schwickert, J.-U. Thiele, and M. F. Doerner, IEEE Trans. Magn. **36**, 10 (2000).
[23] W. Yang, D. N. Lambeth, and D. E. Laughlin, J. Appl. Phys. **85**, 4723 (1999); H. Gong, W. Yang, M. Rao, D. E. Laughlin, and D. N. Lambeth, in *MRS Symposia Proceedings*, Vol. 562 (Materials Research Society, Warrendale, PA, 1999), pp. 27.
[24] O. Idigoras, P. Vavassori, J. M. Porro, and A. Berger, J. Magn. Magn. Mat. **322**, L57 (2010).
[25] J. Hamrle, S. Blomeier, O. Gaier, B. Hillebrands, R. Schäfer, and M. Jourdan, J. Appl. Phys. **100**, 103904 (2006).
[26] F. Scheurer, R. Allenspach, P. Xhonneux, and E. Courtens, Phys. Rev. B **48**, 9890 (1993).
[27] B. N. Engel, M. H. Wiedmann, R. A. VanLeeuwen, and C. M. Falco, Phys. Rev. B **48**, 9894 (1993).
[28] F. Schreiber, Z. Frait, T. Zeidler, N. Metoki, W. Donner, H. Zabel, and J. Pelzl, Phys. Rev. B **51**, 2920 (1995).
[29] M. Cougo dos Santos, J. Geshev, L. G. Pereira, M. C. M. Alves, J. E. Schmidt, and P. Allongue, Phys. Rev. B **70**, 104420 (2004).
[30] These simplifications are not necessary and do not change the observed physical behavior significantly, but they do simplify the mathematics and enhance the transparency of the results.
[31] Our quantitative Kerr microscopy analysis of the magnetization distribution widening is not directly comparable to the anomalous remanent magnetization values that we observe along the nominal *HA* in the same sample, simply because optical microscopy can only see the long-wavelength nonuniformity contributions, which have to be smaller than the total nonuniformity that corresponds to the measured remanent magnetization.